33RD INTERNATIONAL COSMIC RAY CONFERENCE, RIO DE JANEIRO 2013
THE ASTROPARTICLE PHYSICS CONFERENCE

Evidence of optical anisotropy of the South Pole ice

THE ICECUBE COLLABORATION[1]

[1]*See special section in these proceedings*

dima@icecube.wisc.edu

Abstract: In our continued investigations of the optical properties of the South Pole ice, the IceCube collaboration has discovered evidence of a slight azimuthal dependence of the light propagation properties, which can be attributed to an apparently smaller amount of scattering in one preferred direction. We developed a phenomenological model of such anisotropic scattering and fitted it to in-situ light source data. The fitted model significantly improves the description of the calibration data. We have also observed evidence of the anisotropy in the bulk of the muon data and in high-energy cascade neutrino candidate events.

Corresponding authors: Dmitry Chirkin[1]
[1] *Dept. of Physics and WIPAC, University of Wisconsin, Madison, WI 53706, USA*

Keywords: South Pole ice, photon propagation, ice anisotropy.

1 Introduction

IceCube is a cubic-kilometer neutrino detector installed in the ice at the geographic South Pole [1] instrumenting depths between 1450 m and 2450 m. Detector construction started in 2005 and finished in 2010. Neutrino reconstruction relies on the optical detection of Cherenkov radiation emitted by secondary particles produced in neutrino interactions in the surrounding ice or the nearby bedrock.

The optical properties of ice surrounding the detector are described with a table of absorption and effective scattering coefficients describing average ice properties in 10 m-thick ice layers. These properties were determined with a dedicated calibration measurement as described in [2]. The data for this measurement were collected in 2008 with the 40 string detector configuration shown in figure 1. Every optical sensor (digital optical module, or DOM) on string 63 was operated in "flasher" mode to emit light from on-board LEDs in an approximately azimuthally-symmetric pattern, which was observed by the DOMs on the surrounding strings.

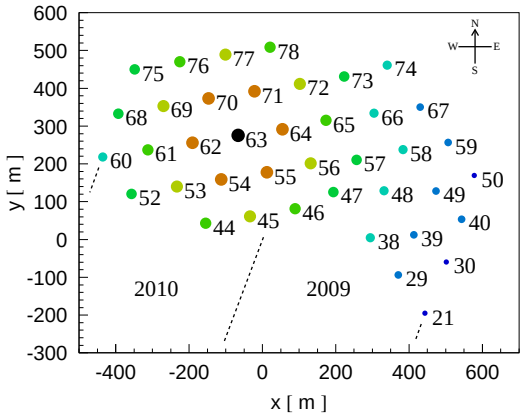


Figure 1: Top view layout of IceCube in the 40-string configuration in 2008. String 63, for which the DOMs emitted flashing light in the study presented here, is shown in black. The nearest 6 strings are shown in brown. The dashed lines and numbers 2009 and 2010 in the left figure indicate the approximate location of the detector parts deployed during those years.

2 Anisotropy of South Pole Ice

Shortly after the study of [2] was complete, we noticed a consistent azimuthal asymmetry in charge collected on the strings surrounding the flashing string that depends on the direction and distance to receiving string. Figures 2, 3, and 4 demonstrate the observed effect: more light is observed in the direction of strings 70 and 55 than on average over all directions, by on average about 16% per 100 m of distance from the emitting string 63.

It appears that the in-situ light source data collected by IceCube contains evidence of ice anisotropy, i.e., different photon propagation properties in different directions of the *xy* plane. It additionally appears that these properties are, to a large extent, the same in the directions $\vec{n}$ and $-\vec{n}$ for any $\vec{n}$ in the *xy* plane. This observation is important as it precludes a possibility that the location of the hole ice (ice re-frozen after the string deployment or otherwise impacted by the deployment) or the supporting cable with respect to the DOMs can create the effect present in data. It it is highly unlikely that any effect from the hole ice or the cable would have a consistent directional behavior for all the DOMs on the emitting string and for all receiving strings. Therefore, we must ascribe the observed effect, to at least some extent, to the inherent properties of the surrounding ice.

Although one can calculate the scattering and absorption properties of individual dust particles, whatever their shape, the positions and orientations of all dust particles at any depth in the volume of the detector are unknown. Perhaps the observed effect is caused by the preferential alignment of the ice crystals, possibly resulting in the preferential alignment of the embedded dust particles. The microscopic cause of the observed effect being unknown we nevertheless note that it should be possible to specify the

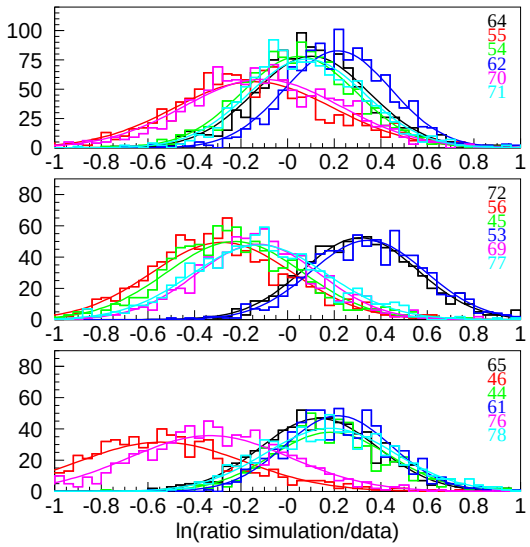


Figure 2: Ratio of simulation to data of total charge collected in DOMs on strings surrounding string 63: nearby strings 64, 55, 54, 62, 70, and 71 ($\sim$ 125 m away), next-to-near strings 72, 56, 45, 53, 69, and 77 ($\sim$ 217 m away), and even further ring of strings 65, 46, 44, 61, 76, and 78 ($\sim$ 250 m away). Each histogram contains entries for all emitters on string 63 and receivers on the denoted string such that the total received charge is greater than 10 p.e. The ice model used in simulation is that of [2] and lacks anisotropy.

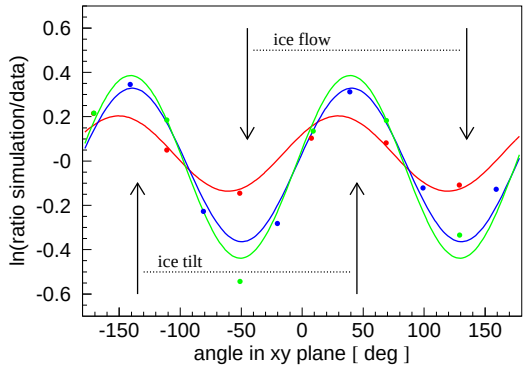


Figure 3: The maxima of histograms in figure 2 is plotted vs. azimuth of the direction from the emitting string 63 to the corresponding receiving strings. The points approximately fall on the fitted sines of twice the azimuth angle with phase that is approximately the same for all 3 curves and amplitude that increases with distance to the corresponding strings ($\sim$ 125 m, 217 m, or 250 m). Also shown are the gradient direction of the ice tilt (see [2]) and direction in which the ice moves at the South Pole at a rate of about 10 m/year (ice flow).

anisotropic properties of ice in some useful macroscopic way.

One naive approach is to specify that the scattering coefficient depends on the photon direction in the xy plane as $b_e(\vec{n}) = b_e \cdot \varsigma(\phi)$, where ϕ is the azimuth angle of the photon direction $\vec{n}$. We, however, note, that this alone will not lead to a consistent description of the

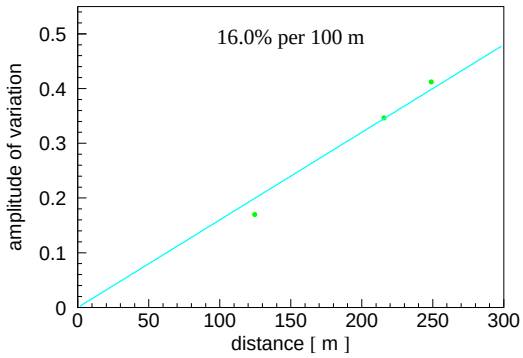


Figure 4: The amplitudes of sines fitted in figure 3 vs. distance. The 16% per 100 m fitted here describes the average behavior at all depths in the detector. This value, when computed for various depths, ranges from 10% in the clearest ice to 23% at the top of the detector.

observed ice properties as the following relationship on the scattering cross section is not satisfied: $\sigma(\vec{n}_{in}, \vec{n}_{out}) = \sigma(\vec{n}_{out}, \vec{n}_{in})$. This relationship follows from combining the generic time-reversal symmetry condition $\sigma(\vec{n}_{in}, \vec{n}_{out}) = \sigma(-\vec{n}_{out}, -\vec{n}_{in})$ and the $\vec{n} \leftrightarrow -\vec{n}$ symmetry that we noted earlier: $\sigma(\vec{n}_{in}, \vec{n}_{out}) = \sigma(-\vec{n}_{in}, -\vec{n}_{out})$ (that we generalized here to all directions for all microscopic scattering events).

The following description is what we decided to use, and it is consistent with the above condition on the cross section. Instead of modifying the scattering coefficient b_e, we modify the scattering function $f(\cos\theta)$ instead:

$$f(\vec{n}_i \cdot \vec{n}_o) \to f(\vec{k}_i \cdot \vec{k}_o), \quad \vec{k}_{i,o} = \frac{A\vec{n}_{i,o}}{|A\vec{n}_{i,o}|}.$$

The matrix A can be diagonalized to

$$A = \begin{pmatrix} \alpha & 0 & 0 \\ 0 & \beta & 0 \\ 0 & 0 & \gamma \end{pmatrix} = \exp \begin{pmatrix} \kappa_1 & 0 & 0 \\ 0 & \kappa_2 & 0 \\ 0 & 0 & \kappa_3 \end{pmatrix}$$

in a basis of the direction of the largest scattering in the xy plane, the direction of the smallest scattering in the xy plane, and z. If the ice is isotropic, $\alpha = \beta = \gamma = 1$, and we get back the scattering function that only depends on a product $\vec{n}_i \cdot \vec{n}_o$. If there is anisotropy we can always assume that $\alpha\beta\gamma = 1$ (or $\kappa_1 + \kappa_2 + \kappa_3 = 0$), since descriptions with a matrix A and cA (c being any number $\neq 0$) are equivalent to each other. This can be seen from the expression for $\vec{k}$, from which c cancels out.

With this description of scattering the geometric scattering coefficient b is constant for all directions, while the effective scattering coefficient $b_e = b \cdot (1 - \langle\cos\theta\rangle)$ receives some dependence on the direction of the incident photon via the direction-dependent term $1 - \langle\cos\theta\rangle$. In the following we derive the small-angle scattering approximation for this term, which clarifies this dependence, and can be useful if we choose to modify the absorption coefficient using the empirical relation $a \propto b_e$.

First, we note that since the scattering function $f(\vec{k}_i \cdot \vec{k}_o)$ depends only on the product $\vec{k}_i \cdot \vec{k}_o$, for the difference $\delta\vec{k} = \vec{k}_o - \vec{k}_i$, the following holds:

$$\langle \delta k^i \delta k^j \rangle = \frac{1-h}{2} \cdot \delta_{ij} - (2g - \frac{3h+1}{2}) \cdot k^i k^j,$$

$$g = \langle \vec{k}_o \vec{k}_i \rangle, \quad h = \langle (\vec{k}_o \vec{k}_i)^2 \rangle,$$

where g is a parameter of the scattering function. In this and the following expressions we omit the index i ="in": $\vec{k}_i = \vec{k}$. The brackets $\langle\rangle$ denote averaging over all possible final directions $\vec{k}_{out}$ after a single scatter with probabilities prescribed with the scattering function. The above relationship can be proven by evaluating it in a basis of $\vec{k}$, and any two vectors, perpendicular to $\vec{k}$ and to each other. In this basis,

$$\vec{k}_i = (0,0,1), \quad \vec{k}_o = (\sin\theta\cos\phi, \sin\theta\sin\phi, \cos\theta) \quad \rightarrow$$

$$\delta\vec{k} = (\sin\theta\cos\phi, \sin\theta\sin\phi, \cos\theta - 1).$$

The averaging over the final directions is performed with integration

$$\int_0^{2\pi} d\phi \int_{-1}^{1} f(\cos\theta) d(-\cos\theta)$$

The off-diagonal terms of $\langle \delta k^i \delta k^j \rangle$ are zero due to integration over ϕ. The diagonal terms evaluate to the expression given above. The trace of $\langle \delta k^i \delta k^j \rangle$ evaluates to $\langle \delta\vec{k}^2 \rangle = \langle (\vec{k}_o - \vec{k}_i)^2 \rangle = 2 \cdot (1-g)$.

We note that

$$\vec{n} = |A\vec{n}| \cdot A^{-1}\vec{k}, \quad \vec{n}^2 = |A\vec{n}|^2 \cdot |A^{-1}\vec{k}|^2 = 1$$

$$\rightarrow \quad \vec{n} = \frac{A^{-1}\vec{k}}{|A^{-1}\vec{k}|} = \frac{B\vec{k}}{|B\vec{k}|}.$$

For brevity we use $B = A^{-1}$. We can now evaluate the derivative

$$\frac{\partial n^i}{\partial k^n} = \frac{\partial}{\partial k^n} \frac{B_{ij}k^j}{\sqrt{B_{kl}k^l B_{km}k^m}} = \frac{B_{in}}{|B\vec{k}|} - \frac{B_{ij}k^j B_{kl}k^l B_{kn}}{|B\vec{k}|^3} =$$

$$\frac{B_{in} - n^i n^k B_{kn}}{|B\vec{k}|}.$$

Now we can evaluate the $\langle \vec{n}_i \vec{n}_o \rangle$ from

$$2 \cdot (1 - \langle \vec{n}_i \vec{n}_o \rangle) = \langle (\vec{n}_o - \vec{n}_i)^2 \rangle = \langle \delta\vec{n}^2 \rangle \approx$$

$$\frac{B_{in} - n^i n^k B_{kn}}{|B\vec{k}|} \cdot \frac{B_{im} - n^i n^l B_{lm}}{|B\vec{k}|} \cdot \langle \delta k^n \delta k^m \rangle.$$

The second term proportional to $k^n k^m$ in the expression for $\langle \delta k^n \delta k^m \rangle$ leads to zero contribution in the above expression. Only the first term proportional to δ_{nm} contributes, resulting in

$$2 \cdot (1 - \langle \vec{n}_i \vec{n}_o \rangle) \approx \frac{B_{in}B_{in} - n^i B_{in} n^j B_{jn}}{|B\vec{k}|^2} \cdot \frac{1-h}{2} =$$

$$(B_{in}B_{in} - n^i B_{in} n^j B_{jn}) \cdot |A\vec{n}|^2 \cdot \frac{1-h}{2}.$$

In the simple case when $B_{ij} = \delta_{ij}$, $\vec{n} = \vec{k}$, and we should get back

$$2 \cdot (1-g) \approx 1 - h.$$

Whether this condition is satisfied depends on the properties of the scattering function near its maximum. For $1-g = 0.1$, (1-h)/2=0.090 for simplified Liu (SL) and (1-h)/2=0.063 for Henyey-Greenstein (HG) scattering functions (see [2] for definitions). As a further approximation, we take this condition for granted, and derive the expression for the $1 - \langle \cos\theta \rangle$, which gives us the directional dependence of the effective scattering:

$$1 - \langle \cos\theta \rangle = (1-g) \cdot \frac{1}{2} \cdot (B_{in}B_{in} - n^i B_{in} n^j B_{jn}) \cdot |A\vec{n}|^2.$$

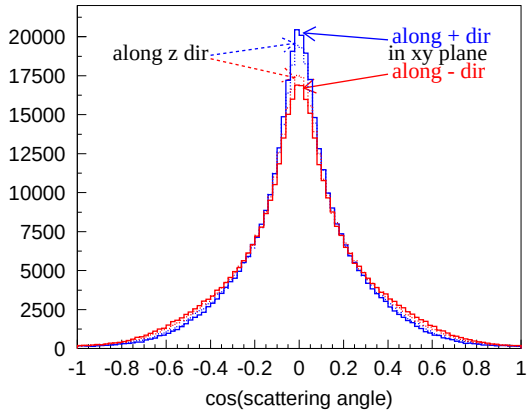


Figure 5: Distributions of the photon direction component after scatter along a direction perpendicular to the initial direction with a -8% anisotropy along the main anisotropy axis ($\kappa_1 = -0.08$). The photons with initial direction along the main anizotropy axis scatter less than the photons with initial directions along the minor axis.

3 Results

We performed fits for the coefficients $\alpha = \exp(\kappa_1)$ and $\beta = \exp(\kappa_2)$ using the two methods of [2]: first, using only the integrated charges on the receiving DOMs and, second, time using the time-binned data. The likelihood description used by the fit was updated according to [3]. The main axes of the diagonalized matrix A describing anisotropy were chosen: one along the z-axis, and the other two in the xy plane. The azimuth angle of the axes in the xy plane was also fitted. The two methods yield anisotropy coefficient values that are within 20% of their average: $\kappa_1 = -0.082$ and $\kappa_2 = 0.040$, as shown in figure 6. Taking these as the result the third coefficient is $\kappa_3 = -\kappa_1 - \kappa_2 = 0.042$.

The 20% error is possibly due to effects unaccounted yet in this fit, such as depth dependence of the anisotropy matrix. Within these errors we can assume that $\kappa_2 = \kappa_3$, and, thus, that there is a symmetry between the to directions described by κ_2 and κ_3, and that that main axis of anisotropy is described by κ_1. The direction of this axis was fitted to 216 degrees. Figure 5 demonstrates the effect of anisotropy on photon scattering in the direction along and perpendicular to the main axis.

We repeated the entire ice model fit procedure described in [2], additionally fitting for the anisotropy (the two coefficients κ_1, κ_2, and the direction of the axis corresponding to κ_1). The resulting absorption and effective scattering are in good agreement with the result reported in [2], as shown in figure 8. The oscillating behavior in the ratio of data to

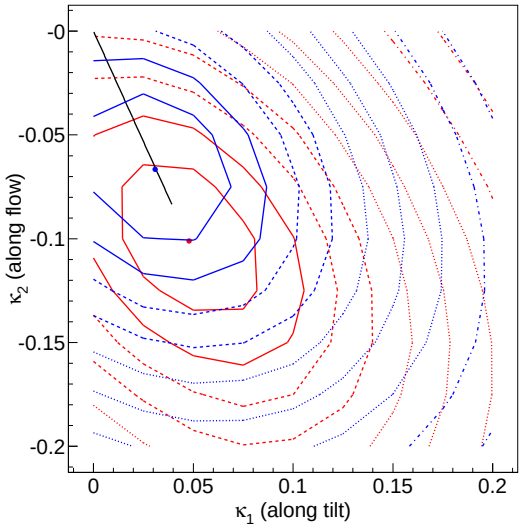


Figure 6: Likelihood function in the vicinity of the minimum using only charge information (red) and using time-binned data (blue). The values are shown with contours on a log scale. The two dots in each plot show positions of the minima in both cases. The line is drawn from (0,0) to the average of the two dots and shows that the ratio of κ_2/κ_1 is approximately the same in both cases.

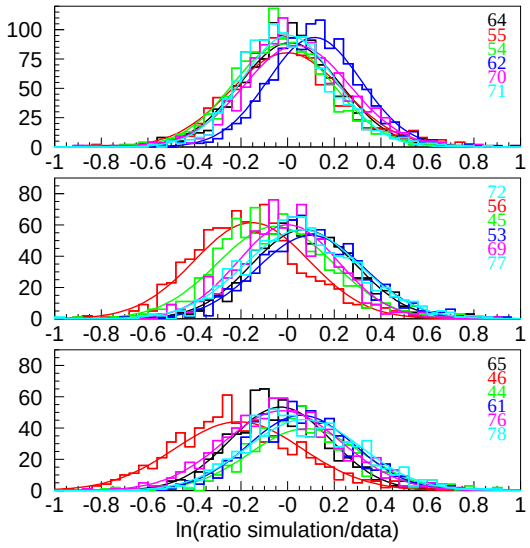


Figure 7: Ratio of (updated) simulation to data of total charges collected in DOMs on strings surrounding string 63, same notations as in figure 2. The ice model used in this simulation includes the anisotropy fit result of this paper.

simulation vs. direction to receiving string is substantially reduced, as shown in figure 7.

The ice anisotropy reported here has also been confirmed with a study that employed well-reconstructed downgoing muons, where the charge collected in a direction of the main anisotropy axis showed an average $\sim 14\%$ excess at 100 m away from the muon with respect to the average over all directions (see figure 9).

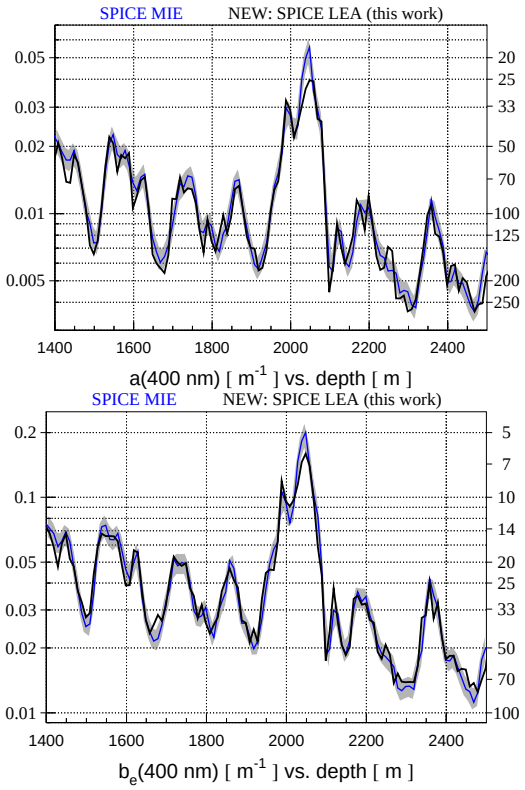


Figure 8: New absorption and effective scattering parameters (LEA) compared with the result reported in [2] (MIE). The grey band around the MIE result shows the uncertainties reported in [2].

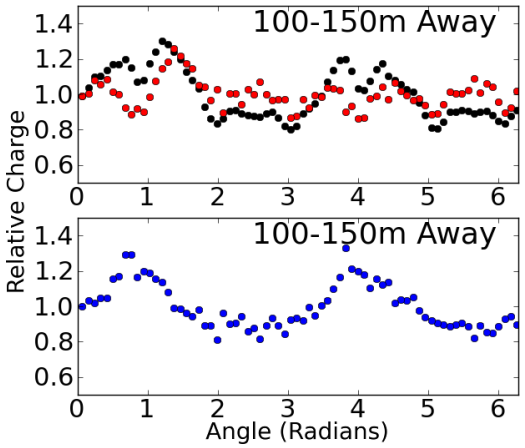


Figure 9: Top: Variations in charge collected 100-150 m away from the reconstructed muon tracks in data (black) and simulation based on ice model of [2] lacking anisotropy (for which some variation is expected due to hexagonal detector geometry). Bottom: ratio of data to simulation curves of the plot above.

References

[1] A. Achterberg et al., Astropart.Phys., 26 (2006) 155.
[2] M. Aartsen et al., NIM-A, 711 (2013) 73, arXiv:1301.5361.
[3] D. Chirkin, arXiv:1304.0735.